INTERNATIONAL JOURNAL OF CLIMATOLOGY
Int. J. Climatol. **32**: 347–363 (2012)
Published online 4 January 2011 in Wiley Online Library
(wileyonlinelibrary.com) DOI: 10.1002/joc.2270

Characteristic 20th and 21st century precipitation and temperature patterns and changes over the Greater Horn of Africa

Richard O. Anyah[a]* and Weini Qiu[a,b]
[a] *Department of Natural Resources and the Environment, University of Connecticut, Storrs, CT 06269, USA*
[b] *Department of Environmental Engineering, University of Connecticut, Storrs, CT 06269, USA*

ABSTRACT: Characteristic patterns and changes in precipitation and temperature over the Greater Horn of Africa during the 20th and 21st century are analysed based on a sample of Coupled Model Intercomparison Project version 3 (CMIP3) models output. Analysis of the 11 CMIP3 models indicates that the equatorial eastern Africa region (including the entire Greater Horn of Africa (GHA)) have been experiencing a significant increase in temperature beginning in the early 1980s, in both A1B and A2 scenarios. All the Atmosphere Ocean Global Circulation Models (AOGCMs) analysed represent the correct mean annual cycle of precipitation, but there is a fairly large spread among the models in capturing the dominant bimodal peaks. In particular, all the models tend to overestimate the peak of the October–November–December (OND) season, while at the same time the peak of the March–April–May (MAM) season tends to be centered on May in the models instead of April as observed. The projected changes and probability distribution of minimum (T_{min}) and maximum (T_{max}) temperatures over the GHA sub-region based on PDFs constructed from daily values showed very diverse distributions for the present (1981–2000) and future (2046–2065; 2081–2100) periods. Whereas in the reference (1981–2000) the probability distribution functions (PDFs) constructed for both T_{min} and T_{max}, and during all the seasons had a near normal (but narrow) distribution, those of the future periods were quite diverse but generally very elongated, with significant shifts toward the positive tail. This generally implies that there is consensus among models and the ensemble mean about high likelihood of increase in extreme warmer T_{min} and T_{max} (more so T_{min}) in the future over the GHA region. Our results also show significant increase in the number of days with T_{min} and T_{max} greater the 2 °C (above 1981–2000 average) by the middle as well as the end of 21st century in both the A1B and A1 scenarios. This is especially so during the June, July, and August (JJA) season where all the 92 days of the season indicate projected minimum temperature to increase by more than 2 °C above the 1981–2000 average by the end of 21st century in both scenarios. Copyright © 2011 Royal Meteorological Society

KEY WORDS climate change; Horn of Africa; precipitation and temperature

Received 27 July 2010; Revised 22 October 2010; Accepted 8 November 2010

1. Introduction

The most recent Intergovernmental Panel on Climate Change (IPCC) projections highlight Africa's unique vulnerability to extreme impacts associated with global climate change (IPCC, 2007). It is also increasingly becoming apparent that behind the ongoing research and debate on climate change (global warming) many parts of Africa are already witnessing dire consequences of erratic climatic conditions that are likely associated with regional climatic changes. In most parts of Africa, agriculture is predominantly rain fed and thus very vulnerable to climatic variability and changes, especially seasonal shifts in precipitation patterns and extreme precipitation events. As a whole, agricultural production and food security in many African countries and regions are likely to be severely compromised by climate change and climate variability. However, it should also be noted that many other non-climate-related stressors also exacerbate the negative impacts associated with climate change in many parts of Africa. Widespread poverty, human diseases, and high population density contribute additional stress on demand for food, water, and livestock forage (Davidson *et al.*, 2003; Shongwe *et al.*, 2010).

Unfortunately, the entire African continent is the least studied region in terms of ecosystem dynamics and climate variability (IPCC, 2001, 2007; Hély *et al.*, 2006; Shongwe *et al.*, 2009) and therefore, the primary mechanisms associated with coupled climate-human-ecosystem changes are not well understood. A comprehensive assessment of the potential impacts of climate change on many of Africa's natural ecosystems is hampered by a current lack of understanding of the fundamental physical and dynamical processes

* Correspondence to: Richard O. Anyah, Department of Natural Resources and the Environment, University of Connecticut, Storrs, CT 06269, USA. E-mail: richard.anyah@uconn.edu

that govern the evolution, variability, and changes in the climate systems of the region and how such changes are likely to impact agro-ecological sectors that directly form the lifeblood for a large population. This is partly due to inadequate observations that can be used for comprehensive empirical analysis of the regional climate systems. Another challenge in understanding low-frequency multi-decadal and centennial climate variability is the vastness and uniqueness of the complex African terrain and climate systems over the eastern, western, southern, and northern portions of the continent.

In general, the climate of the continent is controlled by complex maritime and terrestrial interactions that produce a variety of climates across a range of regions, e.g. from the humid tropics to the hyper-arid Sahel and Sahara deserts (e.g. Christensen *et al.*, 2007). Therefore, understanding how possible climatic regime changes may influence future climate variability is critical. The sharp variability of the African climate in space and time poses yet another challenge in understanding and characterising the uncertainty in the response of regional climate to the global warming and background climate change. This means that at regional and sub-regional scale vulnerabilities, impacts and adaptation options/considerations can vary greatly as well. However, before considering downscaling of the global scenarios, it is necessary to undertake comprehensive analysis of the base Global Climate Model (GCM) projections in order to examine and isolate consistency/inconsistency and uncertainties between model and observed regional variability and changes.

In this study, we focus on the Greater Horn of Africa-GHA (Figure 1). The aim of the present study is to analyse and highlight some of the characteristic patterns and uncertainty in the projected precipitation and temperature changes over the GHA sub-region. The region's vulnerability is amplified by the fact that many of its people's livelihoods are dependent on farming and livestock; two sectors that are especially sensitive to perturbations in the climate system. Climate change is therefore likely to set back development and food production in many of the predominantly agro-based economies of sub-Saharan Africa and particularly the GHA. This will mostly be expressed in form of disruption of regular seasonal patterns over large regions of the continent leading to inadequate food production. Other potentially devastating impacts of climate change over the GHA will be changes in the frequency, intensity, and predictability of precipitation, which will ultimately negatively impact water availability resulting in decline in agricultural production and food shortages as well (WWF, 2006). Observed and projected climate variations and changes (IPCC, 2007) suggest that less precipitation will occur during the climatologically dry seasons and may thus cause more frequent droughts and increased desertification in the place.

In the present study, output from 11 AOGCMs in the CMIP3 archive are analysed to characterise the

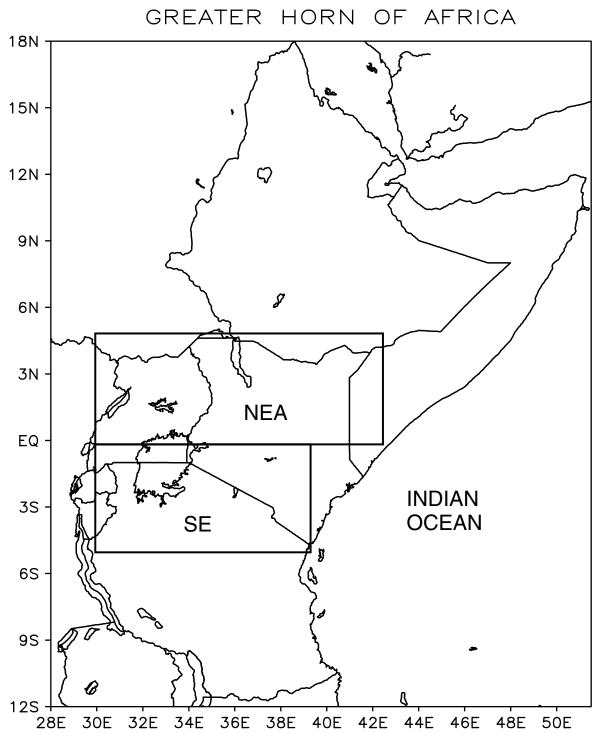

Figure 1. Map of the study area (Greater Horn of Africa), with two regions (North East Africa (NEA), and South East Africa (SEA)) that are utilised for analysis.

projected precipitation and temperature patterns over the GHA sub-region (Figure 1). We focus on the 1971–2000 base period as the control period and the 2046–2100 periods of CMIP3 model projections under the A1B (mid-range) and A2 (high) emissions scenarios. We particularly focus our analysis on 20-year time slices (1981–2000 for present day; 2046–2065 for middle of 21st century projections; and 2081–2100 for end of 21st century projections).

In the following section, we present a brief description of the datasets used. We then present results and discussion beginning with the mean annual cycle from individual and ensemble average of the 11 models derived from the CMIP3 archive. The probability density functions (PDFs) for the control and future projections of temperature and precipitation based on daily temperature data follows, before finally highlighting some of the key results in the summary and conclusion section.

2. Data and analysis

The data used in this study are primarily from 11 GCMs used in the last IPCC, AR4 projections (IPCC, 2007) and derived from the Program for Climate Model Diagnosis and Inter-comparison (PCMDI) archive (www.pcmdi.llnl.gov). We analysed 20th century simulations as well as projections under the A2 and A1B scenarios, which are the IPCC (AR4) high and mid-range CO_2 emissions scenarios, respectively. The projection

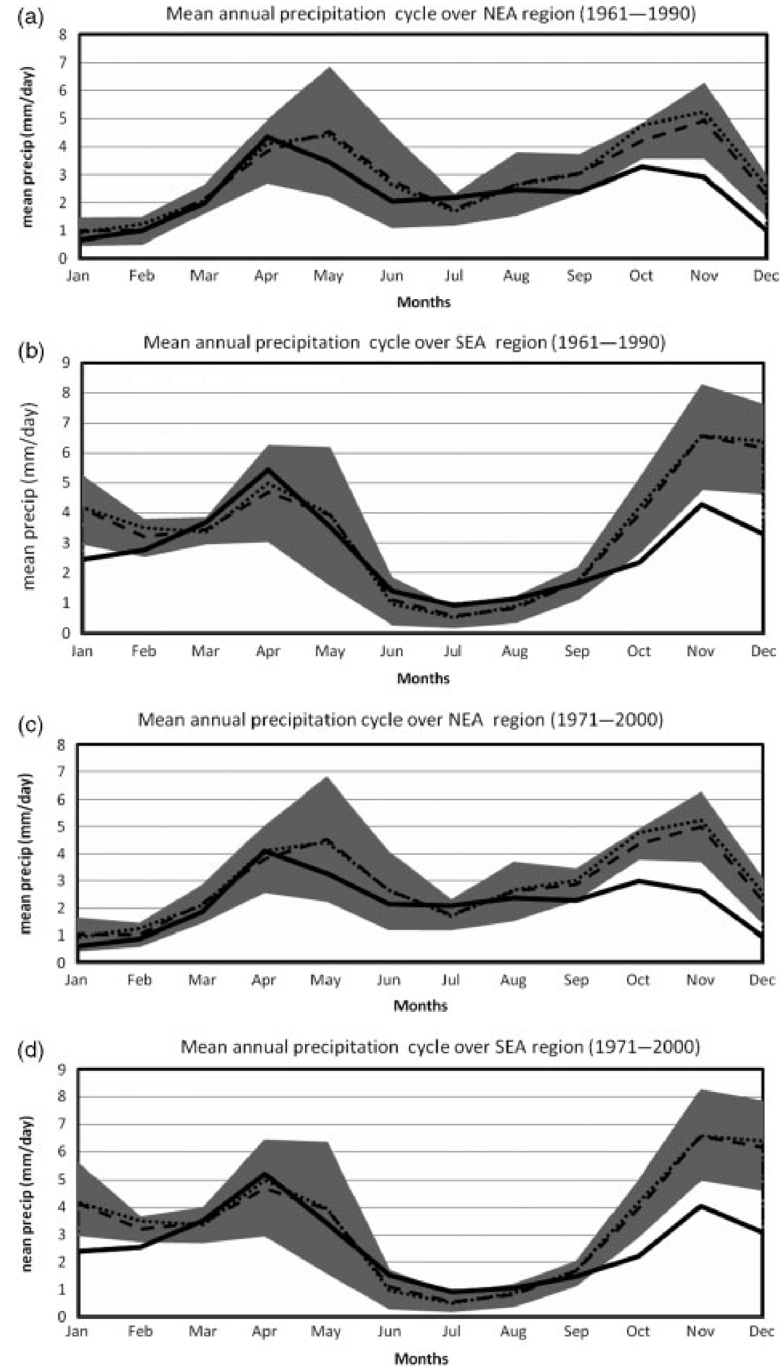

Figure 2. Mean annual cycle of precipitation over north (NEA) and south (SEA) East Africa. CRU (bold black line), A2 projection 2046–2065 (dashed black line), and A2 projection 2081–2100 (dotted black line).

periods (time slices) analysed are 20 years of the middle of the 21st century (2046–2065) and the last two decades of the century (2081–2100). These are compared with the 20th century simulations and observations during the 1981–2000 period. The choice of the 11 models was mostly based on the availability of data for our analysis periods of interest. For extreme temperature and precipitation events, we also specifically analysed daily data from 5 models for which such data are available. The region of focus as mentioned in the previous section is the GHA sub-region (Figure 1), which is one of the climate change hot-spot areas identified in a recent study by Giorgi (2006a). Observed temperature and precipitation (the Global Precipitation Climatology Project (GCPC) and Climatic Research Unit (CRU) datasets) are analysed and compared with individual models as well as the model ensemble mean. For the control, the analyses are based on two baseline periods (1961–1990) and 1971–2000. The comparison of the two baseline periods is motivated by the fact that some previous studies (e.g. Shreck and Semazzi, 2004; Anyah and Semazzi, 2006) have alluded to the fact that

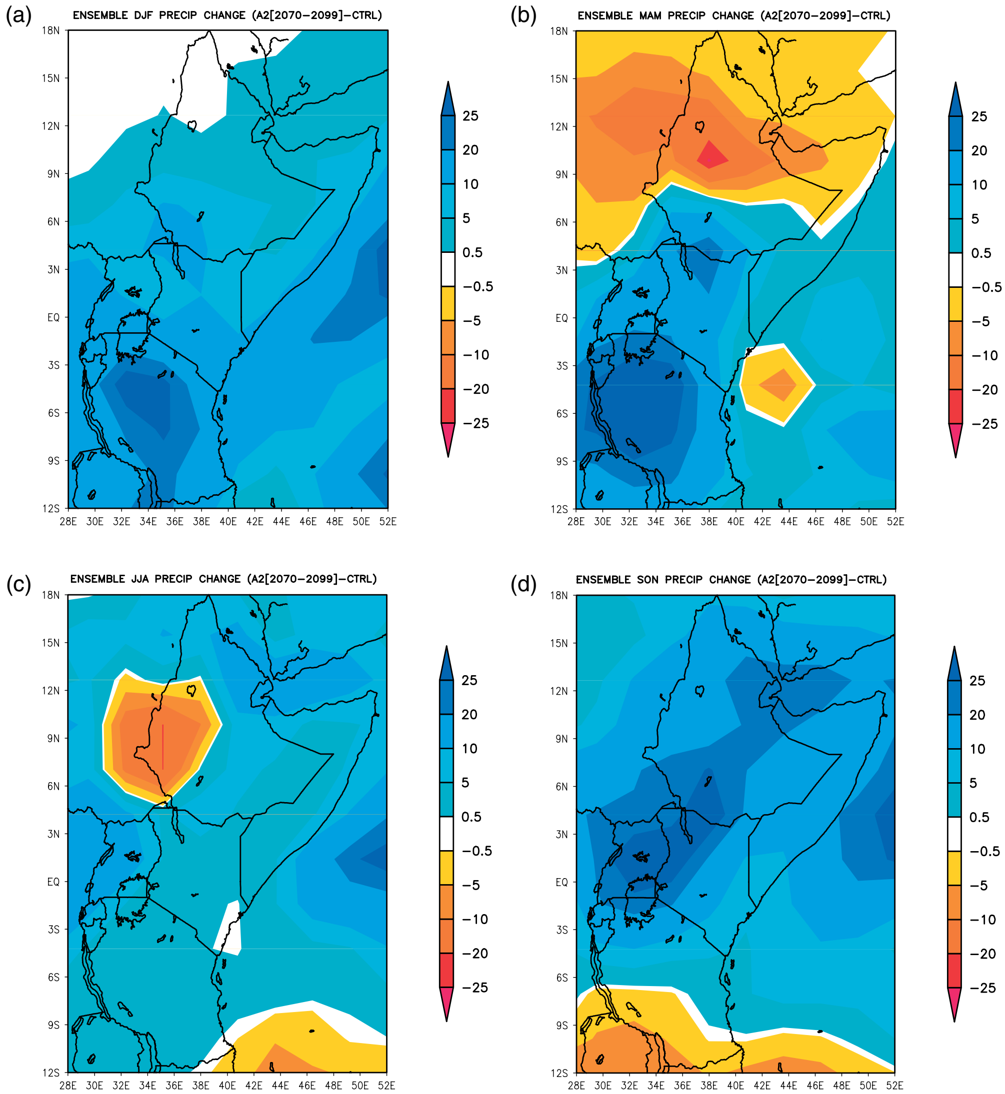

Figure 3. Spatial distribution of precipitation changes between A2 projections at the end of the 21st century and 1961–1990 base period. This figure is available in colour online at wileyonlinelibrary.com/journal/joc

global warming signals on East Africa rainfall and temperature trends tend to be muted during the periods before the middle 1970s. We have also, in some cases, carried out targeted analysis based on 20-year time slices of 1961–1980, 1971–1990, and 1981–2000 reference periods.

3. Results and discussions

3.1. Mean annual cycle and inter-annual variability

All the 11 IPCC AR4 AOGCMs output used in this study represent the correct annual cycle of precipitation over both North East Africa (NEA) and South East Africa (SEA) (Figure 1). The bimodal regimes in the mean annual precipitation cycle associated with the north–south migration of the Inter-Tropical Convergence Zone (ITCZ) is fairly well captured by all the GCMs, but with fairly large spread among the models (Figure 2(a)–(d)) during both peaks; March–April–May (MAM) and October–November–December (OND). More than half the models considered underestimate the magnitude of rainfall peak during the MAM season, and a number of models also overestimate the MAM peak. On the other hand, all the 11 GCMs analysed overestimate the magnitude of the OND season (in the 20th century simulations), compared to observed (CRU) climatology for 1961–1990 as well as the 1971–2000 base periods. The apparent time shift in the peaking of MAM season in May instead of April (observed) is also a conspicuous feature in many CMIP3 simulated (as well as projected) mean annual precipitation cycle. All GCMs tend to overestimate the second rainfall peak that is experienced during October–November–December (OND) season over both NEA and SEA regions. However, nearly all the GCMs analysed capture the correct time evolution of rainfall during the OND season as the peak month of the season (November) in the reference and projections is consistent with what is observed. Overall, all

Table I. Correlation of variation for seasonal mean precipitation in percent (NEA).

Season	Model	A1B (2046–2065)	A2 (2046–2065)	A1B (2071–2090)	A2 (2071–2090)	REF(1981–2000)
DJF	CNRM	58.946	53.160	52.856	61.322	38.200
	CSIRO_MK3.0	40.298	48.269	54.850	41.834	55.734
	GFDL	71.754	38.923	52.770	46.872	72.261
	GISS	13.544	9.928	15.539	12.922	15.542
	MIROC	28.167	37.464	25.646	21.422	33.855
	NCAR_CCSM	27.401	23.339	24.429	21.162	23.999
	UKMO_HADCM3	21.480	25.435	23.382	25.656	16.104
	ENSEMBLE	**34.924**	**32.793**	**35.457**	**32.723**	**30.792**
MAM	CNRM	43.704	38.576	29.766	33.187	37.478
	CSIRO_MK3.0	39.150	41.291	45.407	46.180	44.416
	GFDL	42.847	39.966	29.890	48.190	64.568
	GISS	15.438	15.743	22.482	18.254	10.591
	MIROC	33.125	41.335	17.283	31.612	35.357
	NCAR_CCSM	16.557	11.769	12.976	11.497	12.937
	UKMO_HADCM3	11.872	10.105	21.849	21.691	12.608
	ENSEMBLE	**29.753**	**30.097**	**24.224**	**27.402**	**30.700**
JJA	CNRM	25.447	31.603	21.355	28.676	27.814
	CSIRO_MK3.0	13.466	7.496	8.995	15.934	10.846
	GFDL	23.943	31.800	22.587	25.651	46.542
	GISS	9.649	11.973	17.580	14.054	9.983
	MIROC	11.485	24.994	22.369	19.210	22.467
	NCAR_CCSM	5.469	7.005	1.998	6.960	3.527
	UKMO_HADCM3	32.913	27.129	33.663	26.485	15.295
	ENSEMBLE	**9.193**	**11.869**	**8.682**	**9.665**	**11.667**
SON	CNRM	33.011	28.528	25.851	27.150	32.303
	CSIRO_MK3.0	17.563	21.371	19.067	19.745	19.128
	GFDL	44.954	45.646	42.663	42.295	59.670
	GISS	18.574	19.254	20.931	23.862	13.393
	MIROC	19.530	26.706	22.286	20.773	23.003
	NCAR_CCSM	15.819	13.845	13.296	13.948	15.965
	UKMO_HADCM3	5.572	8.428	9.715	10.802	5.470
	ENSEMBLE	**18.378**	**18.524**	**18.691**	**18.965**	**15.696**

the GCMs represent the peaks of the two primary rainfall regimes experienced over equatorial East Africa quite well.

3.2. Spatial pattern of precipitation and temperature changes

We analysed the spatial patterns in the projected precipitation under A1B and A2 emissions scenarios. Figure 3 shows the spatial changes in precipitation between CMIP3 model control simulations and the A2 scenario projections. Here, we only show the patterns from a small sample of CMIP3 models and the ensemble mean to demonstrate the inter-model differences in the representation of the projected spatial as well as the temporal patterns of precipitation changes over the entire GHA sub-region. The lack of coherent increase or decrease in the middle (2046–2065) and/or during the last two decades (2081–2100) of the 21st century, projected changes under both A1B and A2 scenarios is an apparent feature in the spatial precipitation changes in the all CMIP3 models. However, there is remarkable seasonality in the projected precipitation changes. For, example, during the DJF season there is a slight increase in precipitation over southern parts of Tanzania. The seasonality in the projected precipitation changes appears to be more of a reflection of the dominant influence of the Inter-Tropical Convergence Zone (ITCZ) on the north–south migration of zones of rainfall maxima over the region. For instance, it is apparent that there is significant increase in projected precipitation amounts in the southern parts of the GHA during DJF season, a time when the ITCZ is located at its southernmost position. On the other hand, during MAM when the ITCZ's zonal branch almost lies along the equator the projected increase in precipitation are also mostly co-located with the ITCZ. The same is observed during the SON season. These results, in addition to the seasonality of precipitation changes revealed in our analysis, are consistent with early findings reported in Shongwe *et al.*, (2009).

Tables I and II present seasonal mean coefficient of variation (standard dev/mean × 100%) of precipitation

Table II. Correlation of Variation for seasonal mean precipitation in percent (SEA).

Season	Model	A1B (2046–2065)	A2 (2046–2065)	A1B (2071–2090)	A2 (2071–2090)	REF(1981–2000)
DJF	CNRM	38.942	42.149	32.297	43.272	36.227
	CSIRO_MK3.0	21.118	24.458	25.101	20.214	15.865
	GFDL	32.661	23.427	33.598	35.621	40.759
	GISS	9.597	12.719	9.147	12.235	12.333
	MIROC	6.548	9.550	8.140	2.818	2.022
	NCAR_CCSM	10.486	12.850	12.727	11.391	11.179
	UKMO_HADCM3	10.131	13.754	11.475	13.040	9.238
	ENSEMBLE	**19.773**	**20.901**	**20.194**	**20.143**	**19.376**
MAM	CNRM	23.975	26.224	25.687	21.537	25.410
	CSIRO_MK3.0	7.324	13.483	4.980	11.247	22.309
	GFDL	42.973	40.497	41.437	37.942	4.667
	GISS	18.578	23.867	6.234	21.619	21.387
	MIROC	37.404	31.038	49.893	45.277	28.046
	NCAR_CCSM	37.086	38.949	39.502	35.058	36.858
	UKMO_HADCM3	28.718	26.844	34.750	33.176	14.978
	ENSEMBLE	**21.817**	**21.468**	**22.499**	**21.966**	**15.990**
JJA	CNRM	50.113	38.929	42.897	40.023	33.807
	CSIRO_MK3.0	12.475	26.059	17.810	11.820	26.278
	GFDL	26.314	33.885	28.116	30.031	42.045
	GISS	40.296	40.027	44.452	51.769	39.202
	MIROC	29.228	24.839	26.345	23.153	25.081
	NCAR_CCSM	18.770	24.252	11.929	22.163	7.171
	UKMO_HADCM3	41.890	36.289	34.209	26.592	23.140
	ENSEMBLE	**21.863**	**23.920**	**19.863**	**20.368**	**22.977**
SON	CNRM	58.561	55.902	55.113	56.316	61.306
	CSIRO_MK3.0	67.915	65.646	67.303	69.573	63.632
	GFDL	107.881	102.742	96.236	87.709	109.524
	GISS	59.137	65.377	69.052	67.986	48.690
	MIROC	59.188	57.085	61.758	59.386	46.553
	NCAR_CCSM	48.624	43.209	45.598	41.189	49.010
	UKMO_HADCM3	44.224	44.977	44.358	42.755	40.845
	ENSEMBLE	**62.710**	**59.245**	**61.212**	**60.803**	**58.093**

for NEA and SEA regions, respectively. Coefficient of Variation (CV) has been used and shown in previous studies as a fair measure of precipitation variability since it provides an unbiased estimate of variability for a zero-bounded variable such as rainfall (Raisanen, 2002; Coppola and Giorgi, 2010). In our analysis, for all the seasons (DJF, MAM, JJA, and SON) the CV values are mostly positive in all the projections generated from the 11 models as well as in the Ensemble mean in both reference run and the A1B and A2 emissions scenario projections. Generally, this indicates there is a near-consensus among most AOGCMs about the strong inter-annual variability of precipitation over the GHA.

First, considering the NEA region (Table I), the CV values are higher for the DJF and MAM seasons, and relatively low for the SON season but lowest for the JJA season. For, instance, the DJF CV values derived from all the 11 models analysed ranges between 14 and 90%. The CV values are about 35 and 33% in the ensemble mean by the middle of the 21st century (2046–2065) in A1B and A2 scenarios, respectively. Approximately the same CV values are obtained by the end of the century (2071–2090) in both A1B and A2 scenarios, as well as during the reference period of 1981–2000. The MAM seasonal mean CV values ranges between 12 and 65% among the models, but are about 30% in the ensemble mean by the middle of the 21st century (2046–2065) in the AR4 projections based on both A1B and A2 scenario. On the other hand, the CV values for JJA and SON seasonal mean precipitation are relatively low. In both seasons, the CV values are generally comparable among models and ranges between 2 and 46%, but ranges between 9 and 12% for the JJA and 16 and 19% for the SON in the ensemble mean.

In general, the individual models and the ensemble mean CV values are less than 50% and therefore can be said to meet the dependability criteria threshold (as a measure of inter-annual variability) for seasonal precipitation. This threshold has been proposed as a robust cut-off in some earlier studies (Mishra, 1991). However, the NCAR-PCM1 model was the biggest outlier with computed CV values greater than

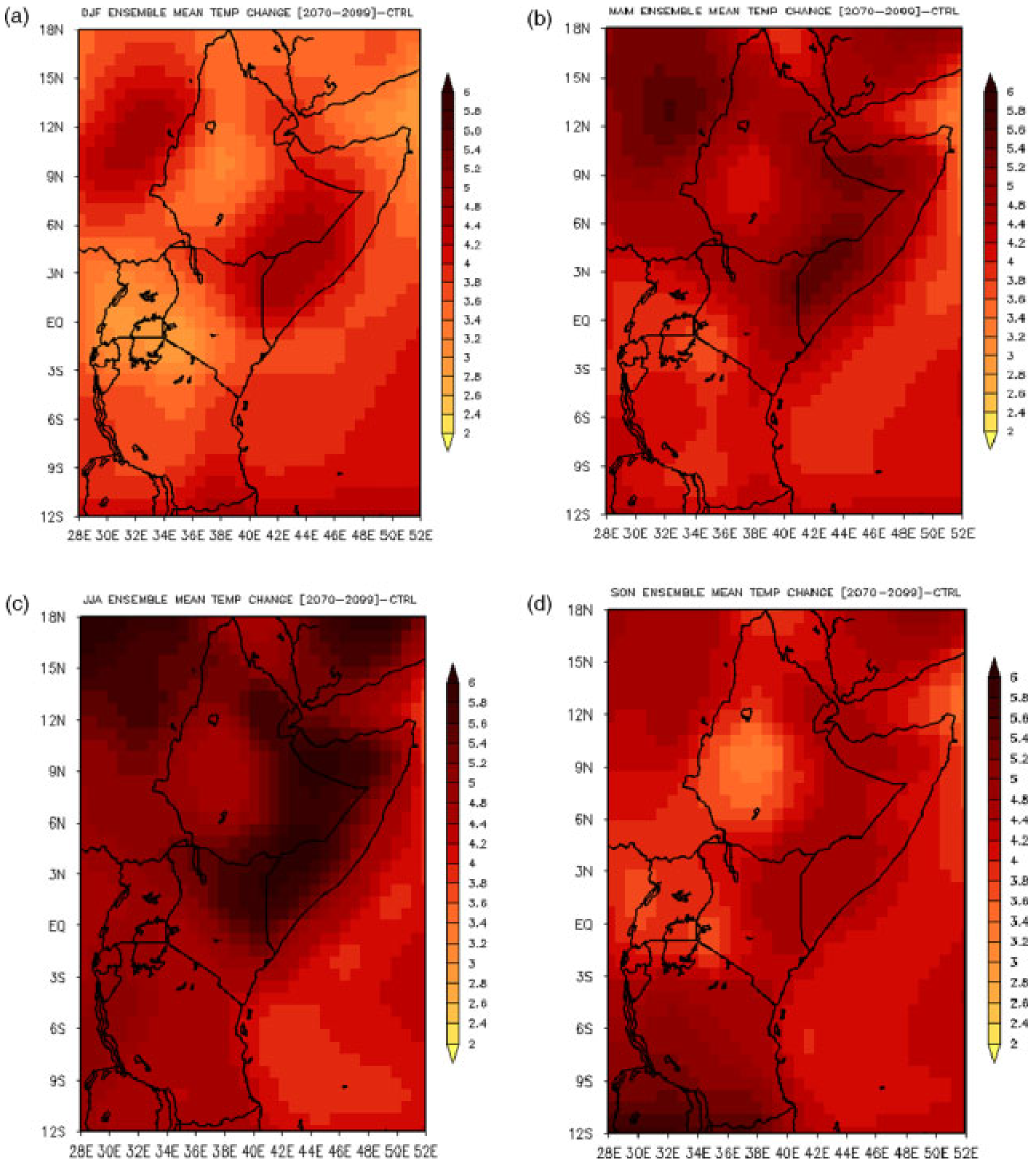

Figure 4. Spatial distribution of mean temperature changes between A2 projections at the end of the 21st century and 1961–1990 base period. This figure is available in colour online at wileyonlinelibrary.com/journal/joc

50% for both A1B and A2 scenario projections during the DJF season. Also based on this, one can say that all the models produce dependable measures of inter-annual variability for the SEA region (Table II), with all CV values in the projections and reference period below 50%. However, the biggest outliers are the GISS, GFDL, and both CSIRO models that produce CV values greater than 50% for the SON season.

Overall, all the models show that there is very strong inter-annual variability during all the four seasons, but particularly during the two primary seasons of MAM and SON (OND). In other words, the projected changes in precipitation in all the 11 models by the middle and end of 21st century show general increase during all the four seasons (Figure II). This seem to be consistent with the climate change hot-spots derived in the Giorgi (2006a) study, where the Horn of Africa is shown as one of the regions where the IPCC AR4 models have a consensus on the sign (+ve) of the projected change in precipitation by the end of the century. However, the results of the present study based on CV as a measure of precipitation variability point to higher likelihood of increased inter-annual variability over the Greater Horn of Africa by the end of the 21st century. This may imply a higher likelihood of more drier-followed-by-wetter cycles in the seasonal precipitation patterns (for example, Mishra (1991).

3.3. Spatial changes in the mean surface temperature and trends

In Figure 4, the spatial distribution of mean surface temperature changes by the end of the 21st century in A2 with reference to the 1961–1990 average depict near uniform increase across the whole of GHA subregion. This is observed during all the seasons, but the

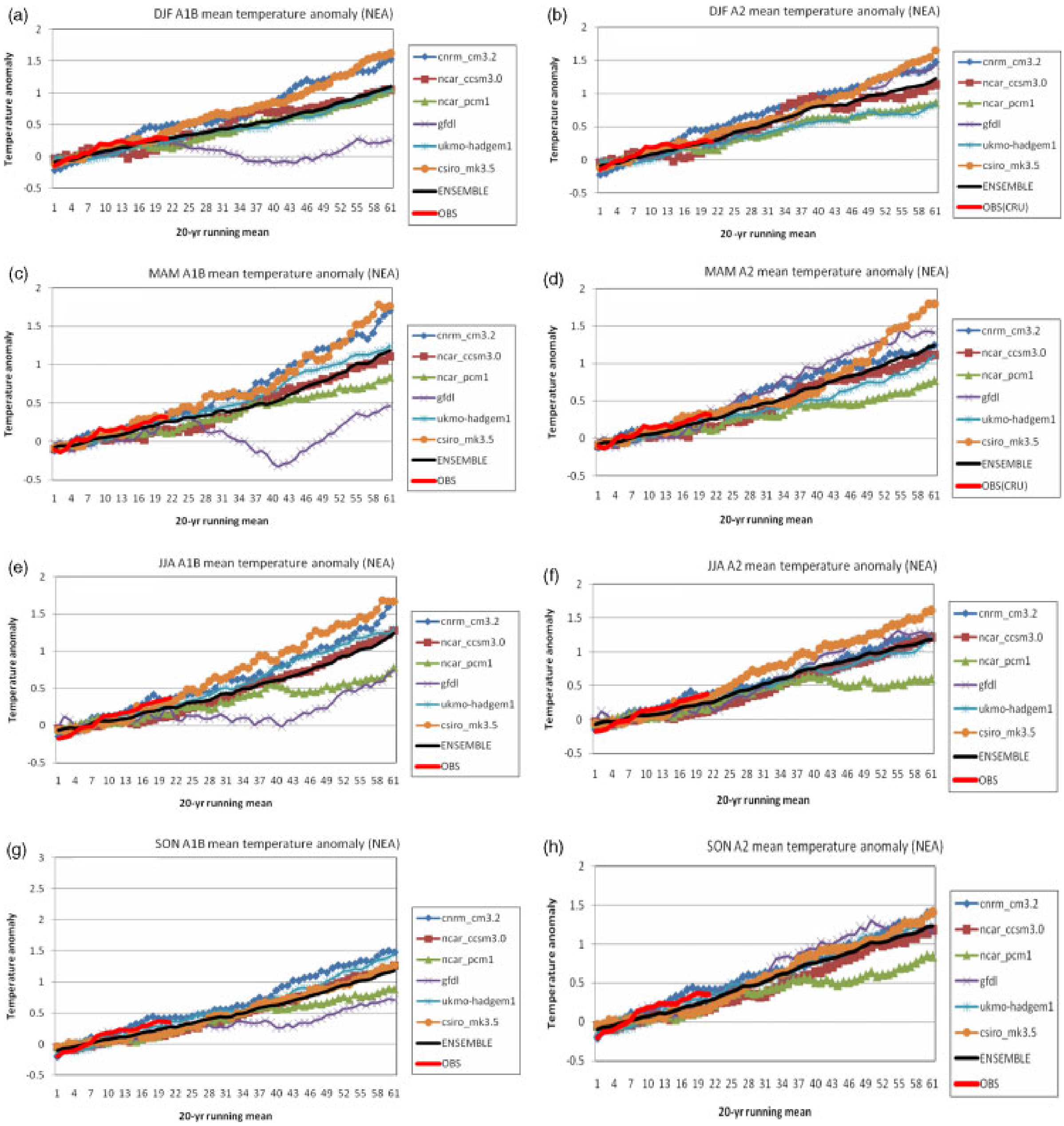

Figure 5. 20-yr running mean of temperature anomaly between A1B and A2 scenario projections and 1981–2000 mean for the period 1961–2040. This figure is available in colour online at wileyonlinelibrary.com/journal/joc

largest warming is projected to occur during the JJA season and concentrated over the northern parts, especially north/northeastern Kenya, western Ethiopia and the whole of Somalia as well as over northern/northeastern Sudan.

In Figure 5, we present trends derived from 20-year running mean of the mean surface temperature anomalies from 1961 to 2040 based on the 1961–1990 average. Here, we only show the results for the NEA region. For all seasons all the six models used in this part of the study present a very consistent increasing trend in the mean surface temperature during all the seasons in both A1B and A2 scenarios. The warming trend in the projected temperature anomaly reaches an average of about 1 °C during DJF, MAM and SON, but a little higher (1.5 °C) during the JJA season by the year 2040 in the A1B scenario. Similarly, the warming trend in the A2 scenario reaches about 1 °C by 2040 during the DJF and SON seasons. The warming consistently increases especially from around 1980, reaching about 2 °C during the MAM and JJA seasons in the A2 scenario (Figure 5(d) and (f)).

4. Projected changes and distribution of maximum and minimum temperature in the 21st century

In this section we discuss the changes in the distribution of seasonal temperature anomalies, with respect

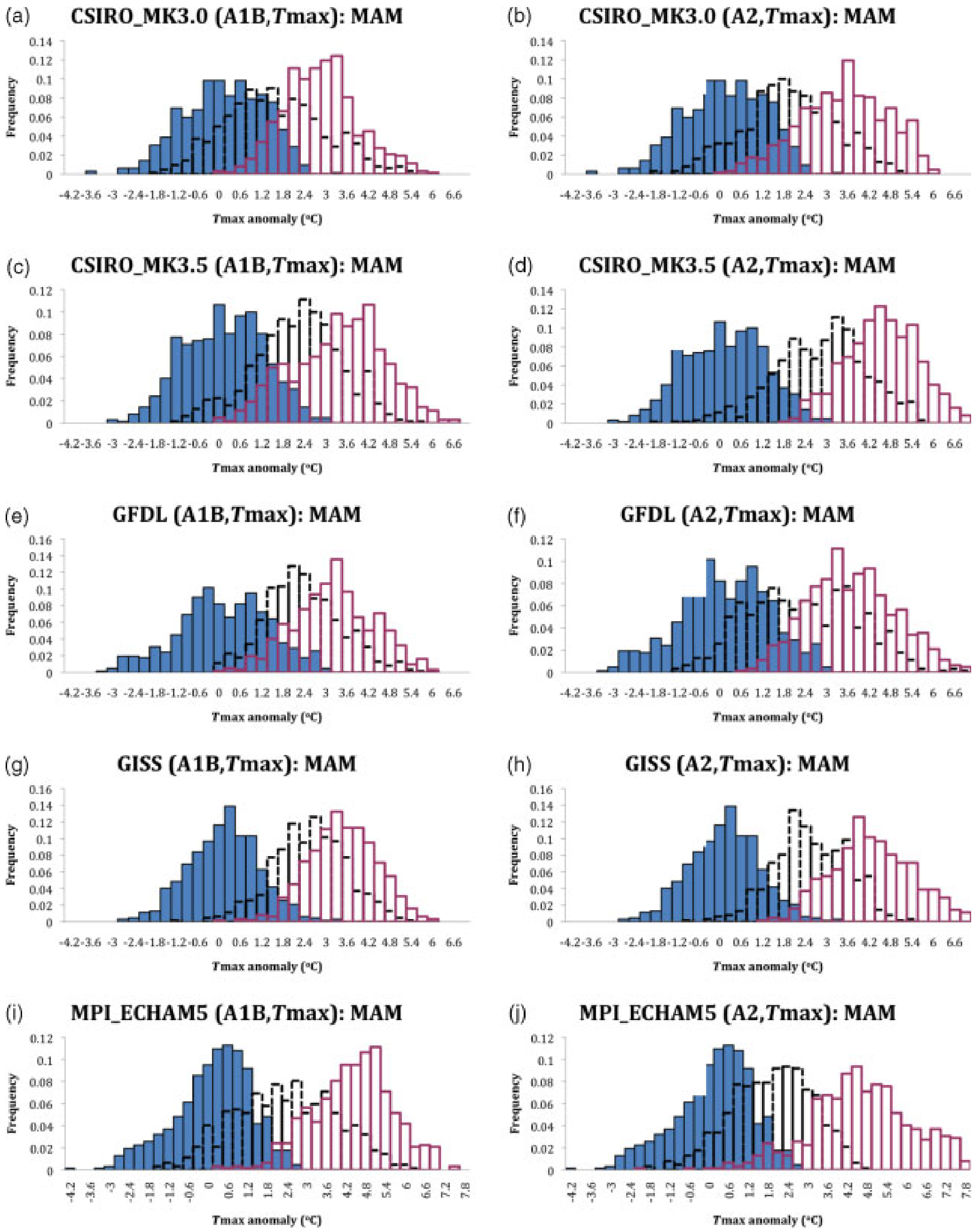

Figure 6. MAM season normalised distribution of mean daily maximum temperature anomalies in a sample of CMIP3 AOGCMs for 1981–2000 (blue), 2046–1065 (black) and 2081–2100 (red) for A1B and A2 scenario projections. This figure is available in colour online at wileyonlinelibrary.com/journal/joc

to the 1981–2000 reference period. The results presented are the probability distribution functions (PDFs) of the projected minimum and maximum temperature changes under the A1B and A2 emissions scenarios for the middle (2046–2065) and end (2081–2100) of the 21st century. We show results from five CMIP3 models for which daily minimum and maximum temperature data were available, for the two primary rainfall seasons, MAM and SON (individual GCMs) and all the four seasons (in the ensemble mean). Note that the PDFs can be utilised in analysing and understanding not only changes in distribution of temperature anomalies, but extremes as well. All seasons show a general increase in both minimum and maximum temperature (in both A1B and A2 scenarios) when compared to the 1981–2000 average from the middle to the end of the 21st century.

During the reference period of 1981–2000 (blue histograms) the PDFs for the DJF season (figure not shown) over NEA region are approximately normal (nearly symmetric) in their distribution shapes. However, the PDFs are also generally narrow during the reference period with exception of the GFDL model, which shows a fairly elongated (broad) distribution. There is consistent and significant broadening of the PDFs for the middle and late 21st century projected changes in both A1B

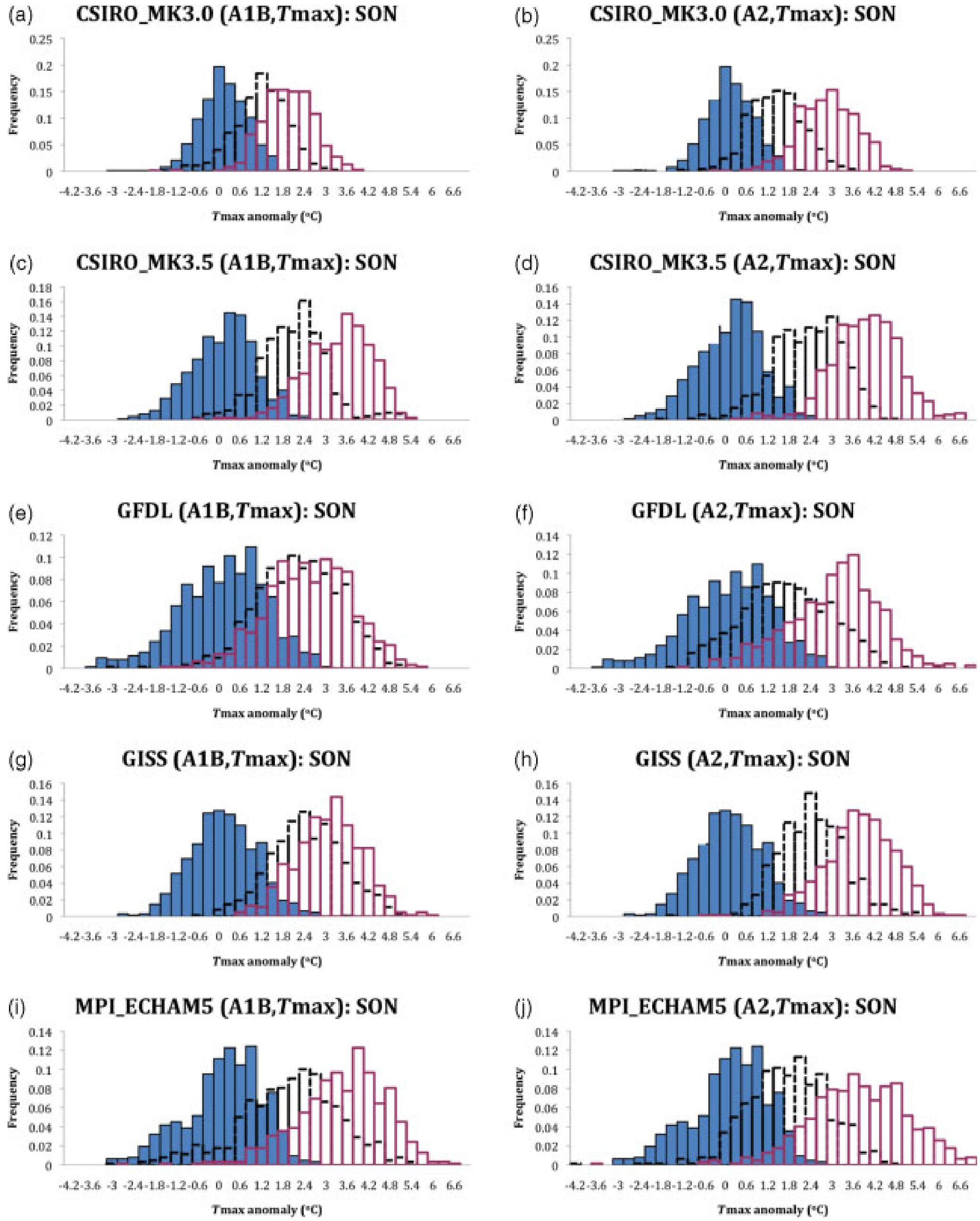

Figure 7. Same as Fig. 6, but for SON season. This figure is available in colour online at wileyonlinelibrary.com/journal/joc

and A2 scenario simulations in all the five models. In general, all the CMIP3 models considered are consistent in representing the spread and distribution of projected changes in T_{max}. This feature is also depicted in the PDFs constructed over the South East Africa (SEA) seasonal T_{max} distribution (not shown). The broadening (especially with a positive skew) of the PDFs in the A1B and A2 scenario projections demonstrates increased likelihood of extreme (warmer) maximum temperatures during the DJF season compared to the 1981–2000 mean.

Similar shifts in the maximum temperature are shown during the MAM season (Figure 6). One outstanding feature is how flat PDFs for the reference period are. The PDFs are even wider/broader for the future periods in both A1B and A2 scenarios. This suggests that there is very large inter-annual variability in T_{max} during the reference (control) period. The flatter PDFs in A1B and A2 emission scenario simulations also imply that future climatic (T_{max}) changes over the GHA are likely to be characterised by more hot (extremely warm) events compared to the 1981–2000 period. This may also suggest that the frequency for days with T_{max} warmer than 1981–2000 normal is likely to be higher by the middle, all the way to the end of the 21st century. The highest projected T_{max} changes in all the models ranges between 5 and 7 °C by the middle (2065) and

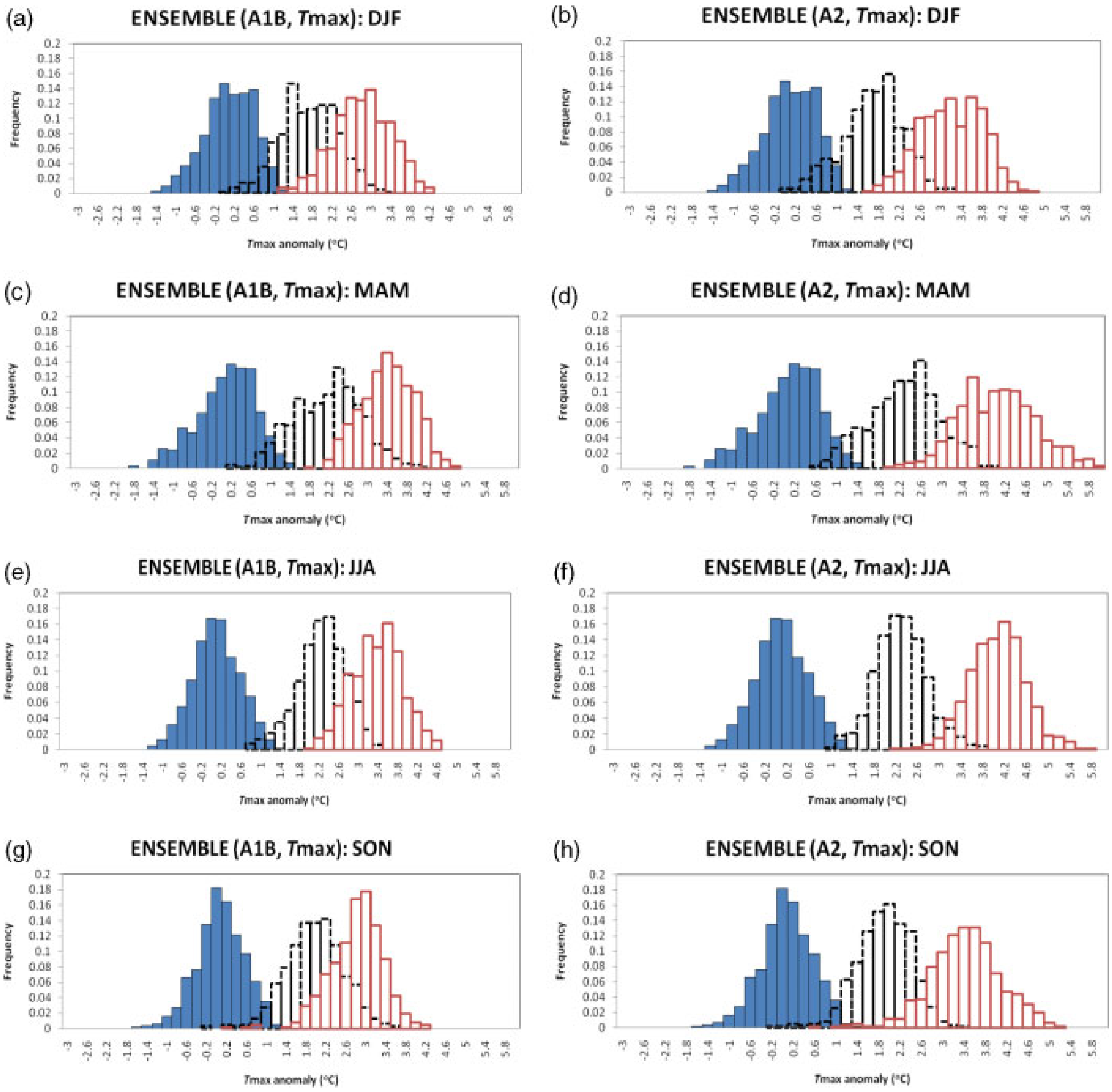

Figure 8. Seasonal normalised distribution of mean daily maximum temperature anomalies in the Ensemble mean of the five CMIP3 AOGCMs for 1981–2000 (blue), 2046–1065 (black) and 2081–2100 (red) for A1B and A2 scenario projections. This figure is available in colour online at wileyonlinelibrary.com/journal/joc

end (2100) of the century in A1B and A2 scenarios, respectively.

Generally, the same characteristic distribution in the changes in T_{max} can be observed in the JJA season (figure not shown) and SON season (Figure 7) and the ensemble mean for all the seasons (Figure 8).

On the other hand, the PDFs of the ensemble mean of minimum temperature (T_{min}) for all the seasons (Figure 9) are shown to be close to normal distribution. However, there is significant shift in the PDFs for future projections in A1B and A2 emissions scenario indicating increased (positive) minimum temperature (T_{min}) anomalies/extremes in the projections from the middle till the end of the 21st century, compared to the 1981–2000 period.

In Figure 10, we present monthly maximum temperature (T_{max}) and minimum temperature (T_{min}) changes based on five CMIP3 models' A1B and A2 projections by the middle and the end of the 21st century compared to the control period (1981–2000). The diagram depicts a 'spider-web'-like shape that clearly shows month-to-month projected T_{max} changes. It is consistently shown in the five models (figure not shown) and their ensemble mean (Figure 11) that the projected change in maximum temperature by the middle of the century compared to the 1981–2000 period is nearly uniform for all the months (between 1 and 2.5 °C) in both A1B and A2 emissions scenario. However, there are very significant month-to-month differences in the amount of projected T_{max} changes in A1B and A2 scenarios by the end of the century. The maximum projected T_{max} change of approximately 4 °C in the A2 scenario seem to occur between the months of April and July, with all the five models showing reasonable consistency in depicting this. The period between October and

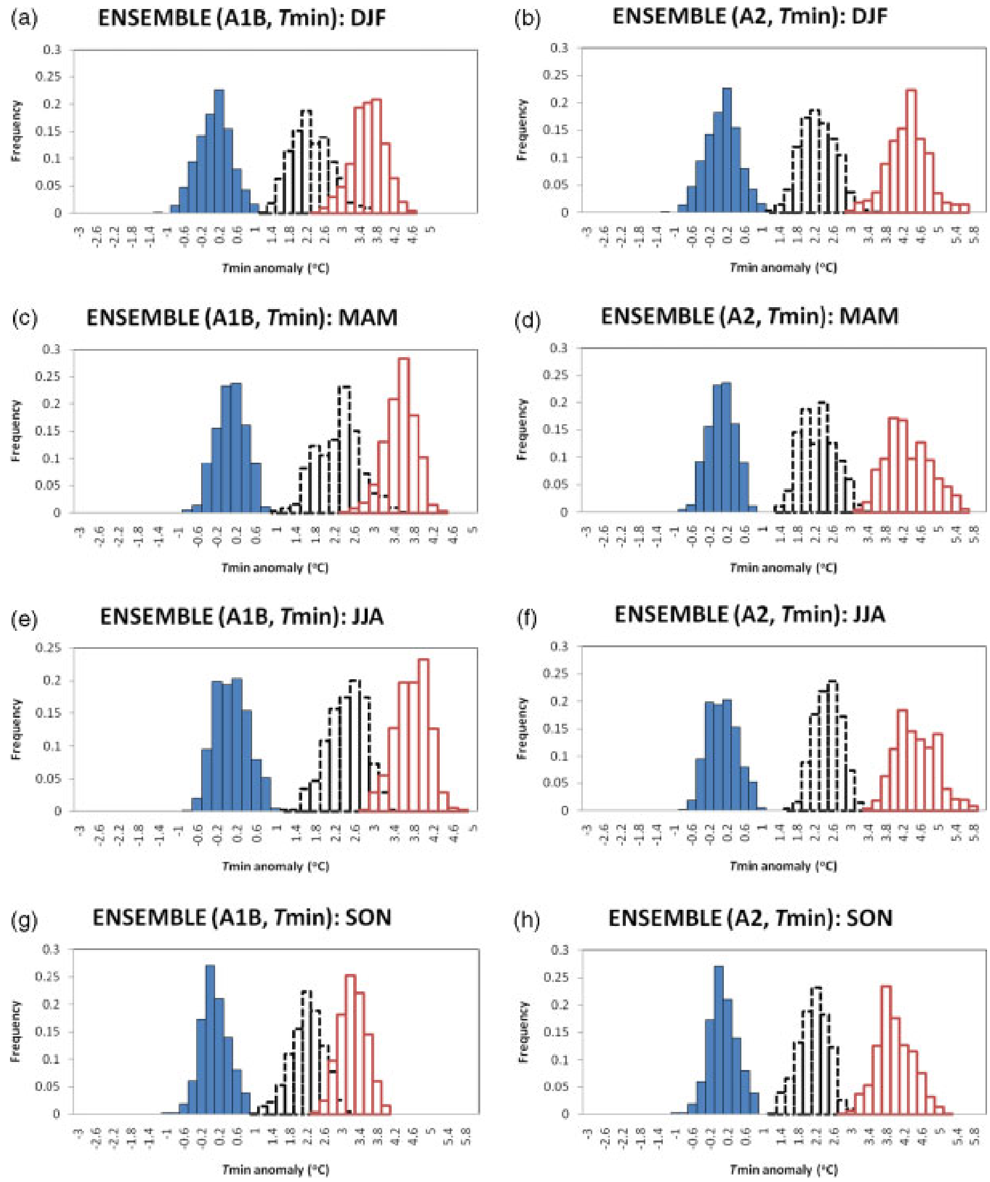

Figure 9. Seasonal normalised distribution of mean daily minimum temperature anomalies in the Ensemble mean of the five CMIP3 AOGCMs for 1981–2000 (blue), 2046–1065 (black) and 2081–2100 (red) for A1B and A2 scenario projections. This figure is available in colour online at wileyonlinelibrary.com/journal/joc

December, on the other hand, is shown to have comparatively least warming of T_{max}, although still significant at an average of 2.5 °C. This feature is consistently shown in most of the individual models analysed, but is even more clearly shown in the ensemble mean (Figure 11).

The spider-web-like diagrams on figure 11 also present T_{min} changes. The two-time periods when the projected change (increase) in minimum temperature is highest: January-March, and May-August are coincident with northern winter and summer periods, respectively. However, there are clear differences (in magnitude) between the changes projected in A1B and A2 by the middle of the century (2046–2065). During May-August, the T_{min} is projected to warm by as much 4.5 °C above the 1981–2000 average by the end of the century in the A2 scenario.

As a whole for all the months, minimum temperatures are projected to significantly increase relative to projected maximum temperature mean surface temperature changes (increases).

5. Probability of days with more than 2 °C change in T_{min} and T_{max}

Figure 12 shows the number of days during the four seasons that exceeded 2 °C above the 20-year mean (1981–2000) as a percentage of the total number of days in each season. The ensemble mean of the five CMIP3 models (for which daily data were available) for the reference period (1981–2000) is compared to the

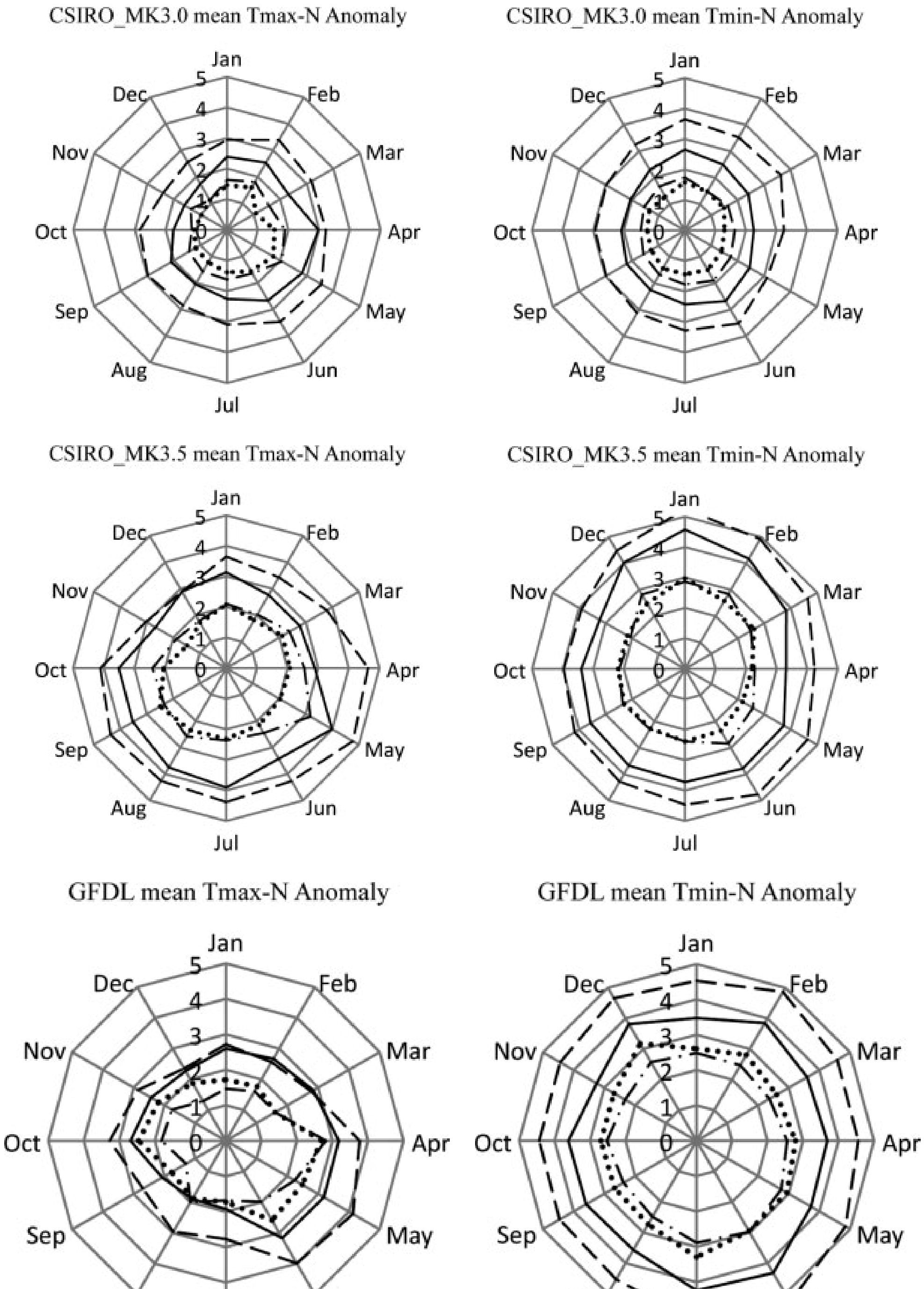

Figure 10. Comparison of T_{max} and T_{min} change based on 1981–2000 average among a sample of CMIP3 models over the NEA region (as in Fig. 1). Left panels are T_{max} and right panels are for T_{min}..

mid-century (2046–2065) and end-of-century (2081–2100) anomalies. During the DJF season, the projected number of days with maximum temperature (T_{max}) warmer than the 20-year mean by 2 °C or more increased from around 20% at the end of 2000 to 30% by 2046, increasing to about 60% by 2065 in the A1B scenario projections (Figure 12(a)) in the northern parts of East Africa. The percentage of days in the A1B and A2 scenario projections for the end of the 21st century (2081–2100) is projected to significantly increase during the last 20 years of the century (Figure 12(a) and (b)). Similar trends are observed for the MAM season (Figure 12(c) and (d)) where by the end of the 21st century the number of days warmer by 2 °C or more above the 1981–2000 mean is almost 100%, meaning that all days of the season are projected to record

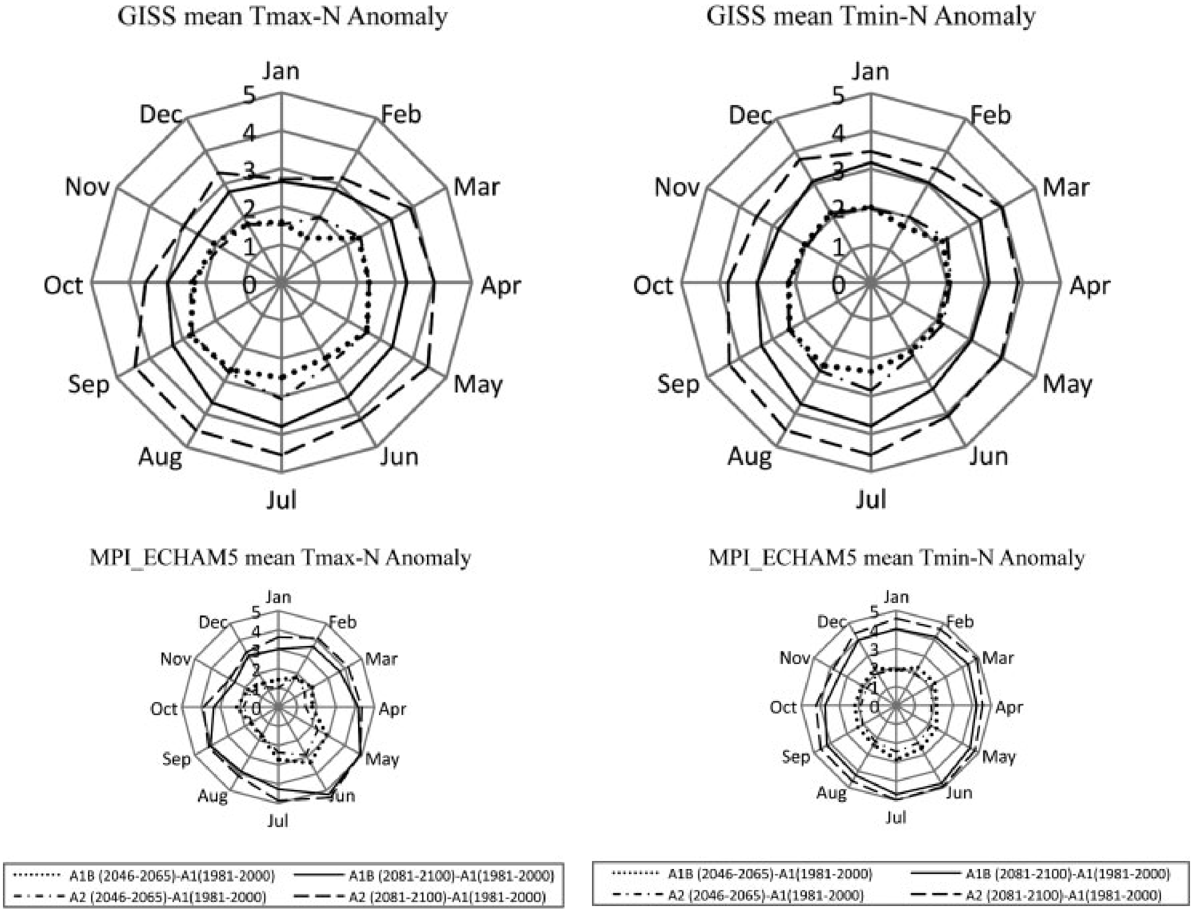

Figure 10. (*Continued*).

minimum temperatures warmer than the 1981–2000 average by more that 2 °C, particularly in the A2 scenario.

During the JJA season (Figure 12(e)) all the 20 years during the 1981–2000 period were not warmer than the 20-year mean by more than 2 °C. However, in both A2 and A1B scenarios most years during the middle and later part of the 21st century are projected to warm considerably (with all days likely to record minimum temperatures warmer than 2 °C above the 1981–2000 average, especially from around the year 2090 to 2100 in both scenarios). Similarly during the SON season (Figure 12(g) and (h)) between 30–50% of days are likely to witness warming of at least 2 °C above the 1981–2000 average by the middle of the 21st century in both A1B and A2 scenarios. The warming is projected to be even larger during the last two decades of the 21st century under both scenarios.

6. Summary and conclusions

In this study, a sample of the CMIP3 models outputs obtained from the PCMDI archive (http://www.pcmdi.llnl.gov) were analysed to synthesise and characterise the temperature and precipitation changes projected to occur over the Greater Horn of Africa (eastern Africa) by the middle and end of 21st century under two emissions scenarios, A1B (mid range) and A2 (high). Overall, the CMIP3 models considered in the present study represent the correct mean annual cycle of precipitation and temperature over both NEA and SEA, but with fairly large spread among the models in capturing the correct peaks of the dominant bimodal precipitation regimes. In particular, most CMIP3 models show late peaking of the long rains season (MAM)-during May instead of April as in observations over equatorial eastern Africa. MAM season is also referred to as the long rains season because this is the period when the region receives the largest fraction of its total annual rainfall. Conversely, though all the models capture the correct peaking of the second primary rainfall season (OND), our analysis also indicated that all the models significantly overestimate the magnitude of the short rains that normally peaks during November in most parts of equatorial eastern Africa.

The 20-year running mean of mean surface temperature anomaly (with respect to 1961–1990 average) from 1961–2040 generally shows a very consistent warming trend (increasing positive temperature anomalies) over both NEA and SEA. There exists a general consensus among the 11 CMIP3 AOGCMs analysed in this study

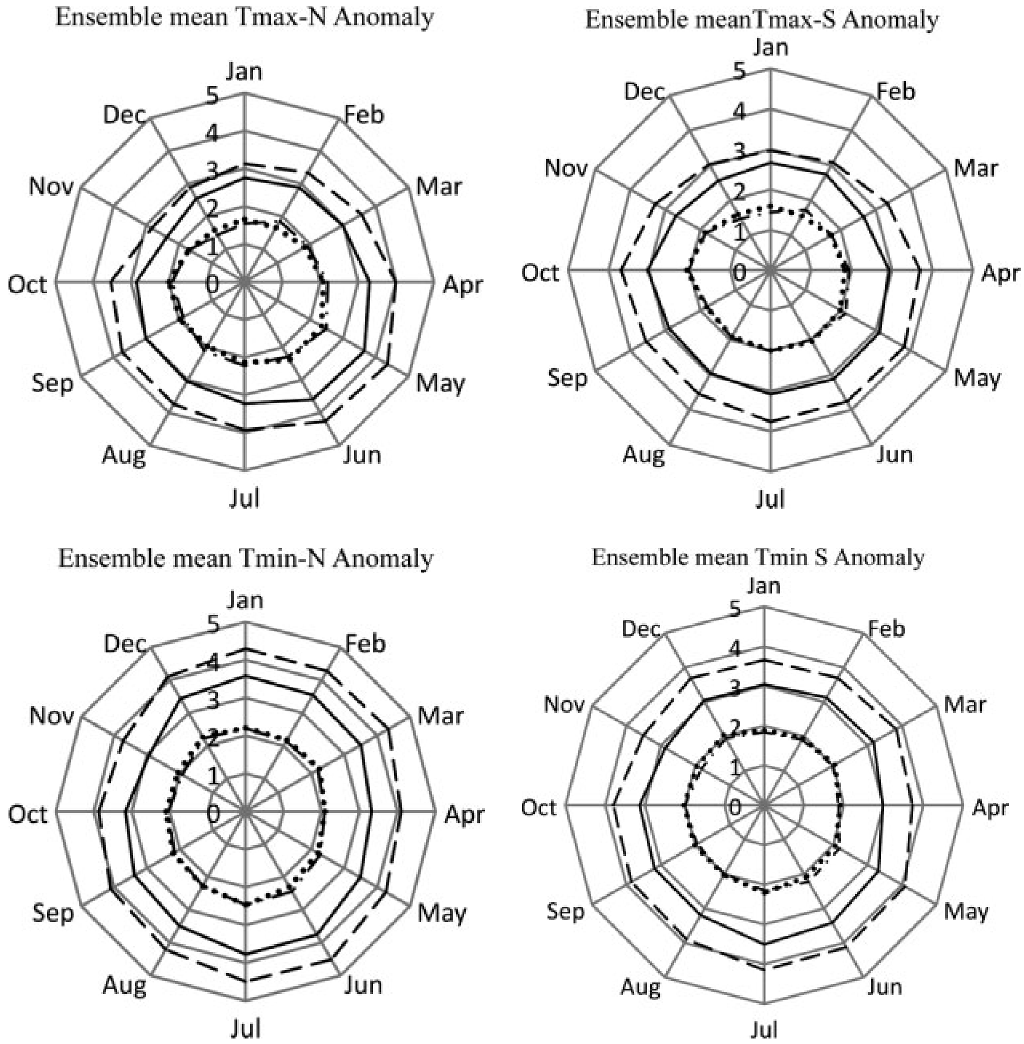

Figure 11. Ensemble mean maximum (T_{max}) and minimum (T_{min}) temperature changes based on 1981–2000 average. (a) T_{max} NEA region, (b) T_{max} SEA region, (c) T_{min} NEA region, and (d) T_{min} SEA region.

on the warming trend of mean surface temperature over the two regions, despite considerable spread in the magnitude of projected increase by the middle of the 21st century (2040) in both A1B and A2 scenarios. Basing on this 20-year running mean the surface temperature is projected to warm between 1 and 2 °C by the middle of the century, especially during the MAM and JJA seasons.

The projected changes and probability distribution functions (PDFs) of minimum and maximum temperatures over the GHA sub-region based on PDFs constructed from daily values showed very diverse distributions for the present (1981–2000) and future (2046–2065; 2081–2100) periods. Whereas during the control period (1981–2000) the PDFs constructed for both T_{min} and T_{max} for all the seasons had a near-normal distribution, those of the future periods were quite diverse though generally having very elongated/broad distributions, also characterised by shift toward the positive tail. This generally implies that there is consensus among models and the ensemble mean about high likelihood of increase in extreme warmer minimum and maximum temperatures in the projections under both A1B and A2 emissions scenarios.

Another unique feature in the temperature projections over equatorial eastern Africa (GHA) is that of the significant increase in the number of days with T_{min} and T_{max} likely to be warmer by more than the 2 °C (above 1981–2000 average) by the middle and end of the 21st century in both the A1B and A1 scenarios. The models analysed tend to have fairly good agreement (near consensus) here. This is especially so during the JJA season although all the other seasons also show significant increase in the number of days with both minimum and maximum temperatures projected to warm by more than 2 °C above the 1981–2000 average.

Acknowledgments

This research was supported by the National Science Foundation (NSF) Grant Number AGS 0805615. Weini

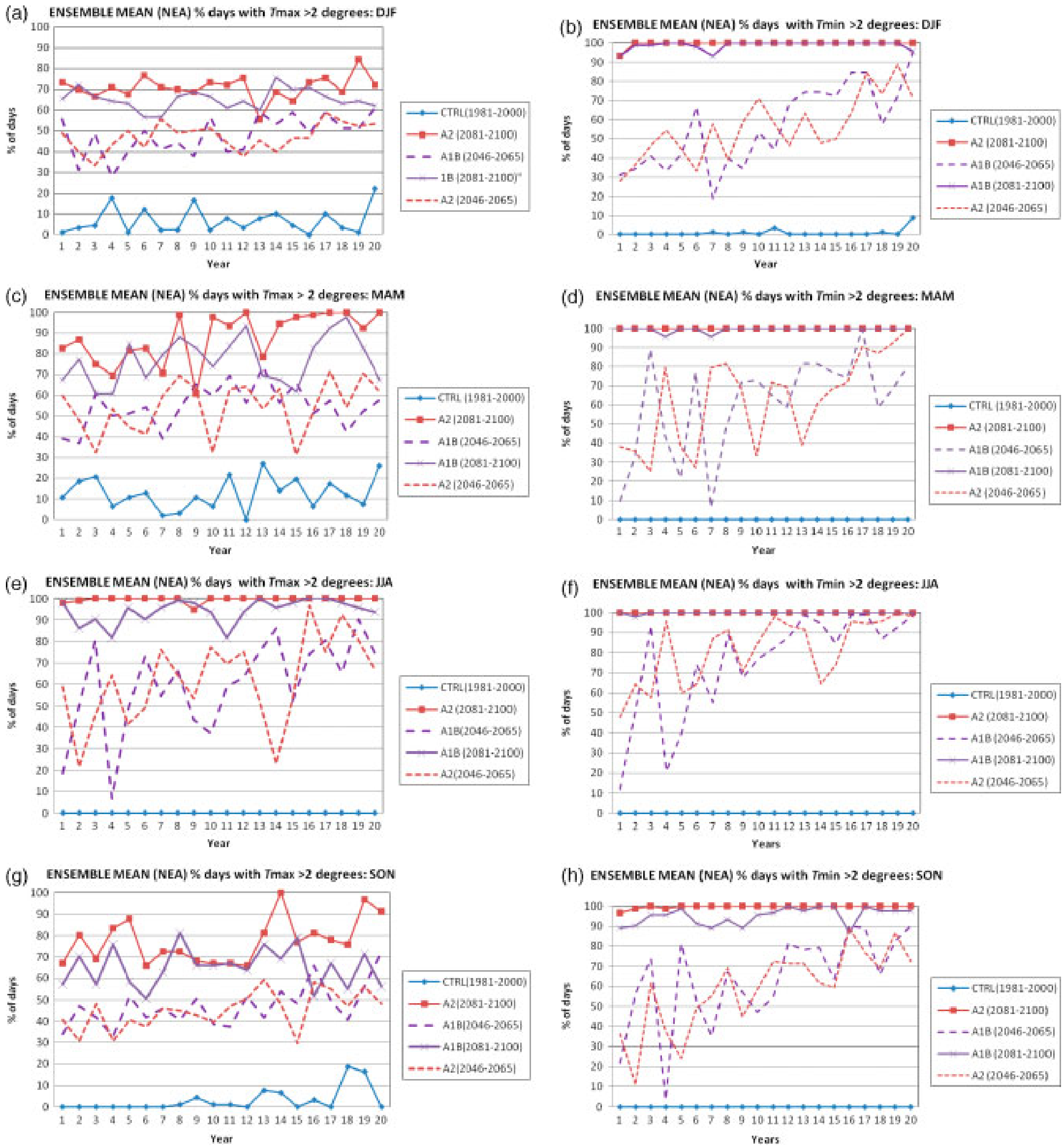

Figure 12. The percent number of days within each season with projected minimum and/or maximum temperature increase by 2° of more during the middle and end 21st century in 1981–2000-based period and A1B and A2 scenario projections. This figure is available in colour online at wileyonlinelibrary.com/journal/joc

Qiu was supported under the NSF-REU Grant provided as supplement to this grant. Finally, we acknowledge the modelling groups, the Program for Climate Model Diagnosis and Intercomparison (PCMDI) and the WCRP's Working Group on Coupled Modeling (WGCM) for their roles in making available the WCRP CMIP3 multi-model dataset.

References

Anyah RO, Semazzi FHM. 2006. NCAR-AGCM ensemble simulations of the variability of the Greater Horn of Africa climate. *Theoretical and Applied Climatology* **86**: 39–62.

Anyah RO, Semazzi FHM, Bowden JH. 2009. Horn of African Regional Climate Model Intercomparison Project (AFRMIP). *CLIVAR-Exchanges* **40**: 3–6.

Christensen JH, Hewitson B, Busuioc A, Chen A, Gao X, Held I, Jones R, Koli RK, Kwon WT, Laprise R, Rueda VM, Mearns L, Menéndez CG, Räisänen J, Rinke A, Sarr A, Whetton P. 2007. Regional climate projections. *Climate Change 2007: The Physical Science Basis. Contribution of Working Group I to the Fourth Assessment Report of the Intergovernmental Panel on Climate Change*, Solomon S, Qin D, Manning M, Chen Z, Marquis M, Averyt KB, Tignor M, Miller HL (eds). Cambridge University Press: Cambridge, pp 847–940.

Coppola E, Giorgi F. 2010. An assessment of temperature and precipitation change projections over Italy from recent global and regional climate model simulations. *International Journal of Climatology* **30**: 11–32.

Davidson O, Halsnaes K, Hug S, Kok M, Metz B, Sokona Y, Verhagen J. 2003. The development and climate nexus: the case of sub-Saharan Africa. *Climate Policy* **3S1**(2003): S97–S113.

Giorgi F. 2006a. Climate Change Hot-spots. *Geophysical Research Letters* **33**: L08707.

Hély C, Bremond L, Alleaume S, Smith B, Sykes TM, Guiot J. 2006. Sensitivity of African biomes to changes in the precipitation regime. *Global Ecology and Biogeography* **15**: 258–270.

Raisanen J. 2002. CO_2-induced changes in interannual temperature and precipitation variability in 19 CMIP2 experiments. *Journal of Climate* **15**: 2395–2411.

Shongwe ME, van Oldenborgh GJ, van den Hurk BJJM, de Boer B, Coelho CAS, van Aalst MK. 2009. Projected changes in mean and extreme precipitation in Africa under global warming. Part I: southern Africa. *Journal of Climate* **22**: 3819–3837.

Shongwe ME, van Oldenborgh GJ, van den Hurk BJJM, van Aalst MK. 2010. Projected changes in mean and extreme precipitation in Africa under global warming. Part II: East Africa. Submitted, *Journal of Climate*.

Shreck CJ, Semazzi FHM. 2004. Variability of the recent climate of eastern Africa. *International Journal of Climatology* **6**: 681–701.

Mishra KK. 1991. Coefficient of variation as a measure of relative wetness of different stations in India. *International Journal of Biometeorology* **34**: 217–220.

IPCC. 2001. *Climate Change 2001: Impacts, Adaptation, and Vulnerability*. Contribution of Working Group II to the Third Assessment Report of the Intergovernmental Panel on Climate Change. McCarthy JJ, Canziani OF, Leary NA, Dokken DJ, White KS (eds). Cambridge University Press: Cambridge, UK, pp 1032.

IPCC. 2007. *Climate Change 2007: Impacts, Adaptation and Vulnerability*. Contribution of Working Group II to the Fourth Assessment. Report of the Intergovernmental Panel on Climate Change ML, Parry OF, Canziani JP, Palutikof PJ, van der Linden, Hanson CE (eds). Cambridge University Press: Cambridge, UK, pp 976.

WWW. 2006. WWF Report on climate change impacts on East Africa.

